Applied Catalysis B: Environmental 225 (2018) 314–323

Contents lists available at ScienceDirect

Applied Catalysis B: Environmental

journal homepage: www.elsevier.com/locate/apcatb

Novel photoactivation promotes catalytic abatement of CO on CuO mesoporous nanosheets with full solar spectrum illumination

Chongyang Zhou, Lei Cheng, Yuanzhi Li*, Min Zeng, Yi Yang, Jichun Wu, Xiujian Zhao

State Key Laboratory of Silicate Materials for Architectures (Wuhan University of Technology),122 Luoshi Road, Wuhan 430070, PR China

ARTICLE INFO

Keywords:
Photocatalytic
CuO mesoporous nanosheets
CO oxidation
Photothermocatalytic
Photoactivation

ABSTRACT

The sample of CuO mesoporous nanosheets (CuO-MNS) was prepared by a facile method of the reaction between NaOH and copper ammonia complex formed from $CuSO_4$ and ammonia aqueous solutions at 25 °C. CuO-MNS shows greatly effective photothermocatalytic activity and excellent durability for the catalytic oxidation of CO (poisonous air pollutant) under the full solar spectrum illumination from a Xe lamp. Compared to commercial nonporous CuO and TiO_2 (P25), the photothermocatalytic activity of CuO-MNS under the Xe lamp illumination is enhanced by 19.8 and 88.7 times, respectively. Under the UV–vis-IR illumination with the same light intensity, the photothermocatalytic activity of CuO-MNS is 331 times higher than its conventional photocatalytic activity. Impressively, CuO-MNS also demonstrates effective photothermocatalytic activity even under the $\lambda > 830$ nm infrared illumination. It is discovered that the greatly effective photothermocatalytic activity of CuO-MNS is attributed to effective solar-light-driven (SLD) thermocatalytic CO oxidation. The significantly enhanced photothermocatalytic activity of CuO-MNS as compared to the commercial nonporous CuO is attributed to the tremendously higher thermocatalytic activity of the former than the later. The results of CO-TPR, Raman, and density functional theory (DFT) calculations reveal that the formation of mesopores in CuO-MNS significantly improves the lattice oxygen activity of CuO, thus significantly enhancing thermocatalytic activity of CuO. Very interestingly, a novel photoactivation, completely unlike the well-known photocatalysis of photocatalytic semiconductors such as TiO_2, is discovered to considerably promote the SLD thermocatalytic CO oxidation on CuO-MNS. By combining the experimental evidence of CO-TPR and O_2-TPO in the dark and under the Xe lamp illumination as well as the theoretical evidence by the DFT calculations in the ground state and excited state, we reveal the origin of the novel photoactivation: the Xe lamp illumination considerably promotes the re-oxidation of the pre-reduced CuO-MNS, thus considerably enhancing the catalytic activity of CuO-MNS.

1. Introduction

Utilization of renewable solar energy for environmental abatement and energy production has been attracting extensive attentions for decades [1–7]. Solar light comprises of 5% UV light, 45% visible light, and about 50% infrared light. The majority of photocatalysts reported are only able to utilize UV or part of visible energy from solar light [1–3]. Hence, developing strategy to design novel effective infrared photocatalysts is very important and great challenging. There have been several strategies developed to design infrared photocatalysts [8,9]. The strategies involve: 1) designing upconversion photocatalyst nanocomposites in which upconversion materials convert the absorbed near-infrared light to UV or visible light that excites UV or visible photocatalysts [10–18], 2) designing plasmonic photocatalysts based on noble metal nanoparticles (e.g. Au, Ag, Pt, Pd, etc.) in which plasmonic hot electrons excited by near-infrared light induce photocatalytic reactions [8,19–23]. 3) designing nanocomposite of semiconductors (e.g. g-C_3N_4) sensitized by near-infrared responsive compounds (e.g. organic dye, zinc phthalocyanine derivative) [24,25], 4) designing near-infrared photocatalysts with bandgap narrow enough to be excited by near-infrared light [9,26–32].

Among the narrow bandgap photocatalysts, nanostructured CuO as p-type semiconductor has attracted interests due to its rich abundance, low cost, and narrow bandgap (1.2 eV in bulk) [33–35]. Various methods have been developed to prepare diverse nanostructured CuO, which exhibited photocatalytic activity for the photodegradation of water pollutants (e.g. dyes) in a batch reaction mode under the illumination of UV or visible light. It has been reported that the photocatalytic activity of nanostructured CuO is affected by several factors such as particle size, surface area, morphology, exposed facets [33,36–42], etc. Photocatalytic reaction on nanostructured CuO follows the well-known photocatalysis mechanism [1–3,33]. Upon the

* Corresponding author.
E-mail address: liyuanzhi66@hotmail.com (Y. Li).

https://doi.org/10.1016/j.apcatb.2017.11.081
Received 12 October 2017; Received in revised form 16 November 2017; Accepted 30 November 2017
Available online 05 December 2017
0926-3373/

illumination of UV or visible light with energy higher than the bandgap of CuO, the electrons in the valence band of CuO are excited to its conduction band. The photogenerated electrons reduce electron acceptors such as O_2, while the photogenerated holes oxidize electron donors such as organic compounds or hydroxyl. Whether the photocatalytic reaction is able to occur on CuO depends on the redox potential of the photogenerated electron low enough to reduce the electron acceptors as well as the redox potential of the photogenerated holes high enough to oxidize the electron donors. Miyauchi et al. [43] have proved that CuO is not an effective photocatalyst in the absence of H_2O_2 due to its inability to produce OH· radicals, which is attributed to the fact that the photogenerated holes in the valence band of CuO has no redox potential necessary for the oxidation of hydroxyl to OH· radicals. Therefore, only the easily degradable dyes with lower redox potential have been reported to be photodegraded on CuO [33–42], thus hindering the wide application of CuO in the photocatalytic environmental abatement. It is highly desirable and great challenging to develop novel catalytic principle different from the well-known photocatalytic mechanism for overcoming the disadvantage of nanostructured CuO as photocatalyst.

Recently, a novel strategy of solar-light-driven (SLD) thermocatalysis, which provides a highly effective method for the abatement of air pollutants by utilizing solar energy, has been developed [44–46]: A catalyst with strong optical absorption in solar spectrum region absorbs solar energy, causing an increase in its surface temperature due to photothermal conversion. When the temperature exceeds the light-off temperature of a thermocatalytic reaction on the catalyst, the thermocatalytic reaction takes place. The reported photothermocatalysts include manganese oxide [44–46], Co3O4[47], Ce1–xBixO2–δ, [48] Pt/LaVO4/TiO2 [49], Pt/CeO2 [50], CuO [51], etc. Some of the photothermocatalysts such as manganese oxide and its nanocomposites exhibit efficient photothermocatalytic activity even under the infrared illumination.[44,45] To our best knowledge, up to now, there have been no reports about the photocatalytic or photothermocatalytic activity of CuO under the infrared illumination. It is not clear whether the photothermocatalytic activity of CuO merely originates from the SLD thermocatalysis.

Herein, we develop a facile method of preparing CuO mesoporous nanosheets (CuO-MNS). CuO-MNS shows greatly effective photothermocatalytic activity for the catalytic oxidation of CO (poisonous air pollutant) under the full solar spectrum (UV–vis-IR) illumination or even under the $\lambda > 830$ nm infrared illumination from a Xe lamp. It is found that the formation of mesopores in CuO-MNS markedly improves the photothermocatalytic of CuO. Compared to commercial nonporous CuO and TiO_2 (P25), the photothermocatalytic of CuO-MNS is enhanced by 19.8 and 88.7 times, respectively. Very interestingly, a novel photoactivation, completely unlike the well-known photocatalysis of photocatalytic semiconductors (e.g. TiO_2), is discovered to considerably promote the SLD thermocatalytic CO oxidation on CuO-MNS. To our best knowledge, up to now, there have been no reports about the photocatalytic or photothermocatalytic activity of CuO under the infrared illumination, and no report about the novel photoactivation on CuO. Under the UV–vis-IR illumination with the same light intensity, the photothermocatalytic activity of CuO-MNS due to the SLD thermocatalysis and the novel photoactivation is 331 times higher than its conventional photocatalytic activity. Based on the experimental evidence of CO-TPR, O_2-TPO, and DFT calculations, we reveal the origin of the significantly enhanced photothermocatalytic activity by the formation of mesopore in CuO and the novel photoactivation on CuO-MNS.

2. Experimental

2.1. Preparation

The sample of CuO mesoporous nanosheets (denoted as CuO-MNS) was prepared according to the procedure as follows: 1.996 g of $CuSO_4{\cdot}5H_2O$ was dissolved into 200 mL of distilled water in a beaker which was placed in a thermostatic water bath at 25 °C. After magnetically stirred for 15 min, 60 mL of 0.15 mol L^{-1} aqueous ammonia solution was dropped in the $CuSO_4$ aqueous solution. After magnetically stirred for 15 min, a blue solution of copper ammonia complex was obtained. Then, 12 mL of 1.2 mol L^{-1} NaOH was dropped into the solution of copper ammonia complex under magnetic stirring. The obtained suspension was magnetically stirred for 24 h in the thermostatic water bath at 25 °C. The obtained black precipitate was filtered, washed with distilled water, and dried in an electric oven at 90 °C.

2.2. Characterization

The crystalline structure of the CuO-MNS sample was determined on a Rigaku D/max diffractometer with Cu Ka radiation. Its morphology was observed on a Hitachi S-4800 scanning electron microscope and a JEM-100CX transmission electron microscope. Its specific surface area and pore volume were measured on an ASAP2020 physisorption instrument using N_2 absorption at −196 °C. Its diffusive reflectance UV–vis-IR absorption spectra were recorded on a Lambda 750 spectrophotometer. Its Raman spectra were recorded on a INVIA Raman microscope using an excitation of 633 nm laser light.

CO temperature programmed reduction (CO-TPR) in a flow of 5 vol % CO/He or O_2 temperature programmed oxidation (O_2-TPO) in a flow of 5 vol% O_2/He of the CuO sample in the dark was performed on a TP5080 multifunctional adsorption apparatus using a quartz tube reactor, of which one end was linked to a quartz window. The setup and measurement procedure were detailed in our previous works [45,52]. The amount of the CuO sample loaded in quartz tube reactor is 0.0100 g. For O_2-TPO, the CuO sample was pre-reduced in a flow of 5 vol% CO/He at 160 °C for 30 min.

To study if the irradiation could affect the CO-TPR or O_2-TPO of the CuO-MNS sample, a CHF-XM500 Xe lamp as light source, which was put in the front of the quartz window of the quartz tube reactor, switched on. In the case, the amount of the CuO-MNS sample was 0.0050 g. The light intensity is 407.42 mW cm^{-2}.

2.3. Photothermocatalytic activity

The photothermocatalytic activity of the CuO sample for CO oxidation was measured on a cylindrical reaction reactor with a quartz window under the irradiation of the Xe lamp. A feed stream of CO concentration of 18.8 g m^{-3}, generated by mixing 20.8 vol% O_2/N_2 and 5 vol% CO/He, was continuously fed into the reactor at a flow rate of 40 mL min^{-1}. The catalyst amount is 0.1000 g. The reactor, the measurement procedure, and the analysis condition of reactant (CO) and product (CO_2) by a gas chromatograph (GC9560) were described in our previous works [41]. To measure the photothermocatalytic activity of the CuO-MNS sample under the visible-infrared (Vis-IR) or infrared (IR) irradiation from the Xe lamp, a corresponding long-wave pass filter was placed in the front of the quartz window of the reactor. The light intensity of the irradiation from the Xe lamp was measured by an optical power meter (Newport 1918-R). The light intensity of the UV–vis-IR, Vis-IR or IR of $\lambda > 420$, 560, 690, or 830 nm is 475.7, 470.2, 451.0, 395.4, 365.8 mW cm^{-2}, respectively.

The photocatalytic activity of the CuO-MNS for CO oxidation at room temperature was measured on the reactor under the irradiation of the Xe lamp according to the procedure reported in our previous work [45].

2.4. Thermocatalytic activity

The thermocatalytic activity of the CuO sample for CO oxidation at different temperature in the dark was measured on a gas-phase reaction apparatus (WFS-2015) using a quartz tube reactor, of which one end

was linked to a quartz window. The amount of the CuO sample loaded in the quartz tube reactor is 0.0500 g. A feed stream with CO concentration of 15.0 g m^{-3}, generated by mixing 20.8 vol% O_2/N_2 and 5 vol% CO/He, was flown into the reactor at a flow rate of 40 mL min^{-1}.

To study if the irradiation is able to affect the thermocatalytic activty of the CuO-MNS sample, the Xe lamp, this was put in the front of the quartz window of the quartz tube reactor, switched on. In the case, the amount of the CuO-MNS sample was 0.0125 g. The irradiation intensity was 517.5 mW cm^{-2}. The setup and measurement procedure were detailed in our previous work [45].

2.5. DFT calculation method

Density functional theory (DFT) calculations were performed to study CuO by using the Perdew–Burke–Ernzerhof functional and projected augmented wave (PAW) pseudopotentials [53,54] which was embedded in the VASP 5.3 Vienna Ab-initio Simulation Package. DFT + U method with a Cu3d U^{eff} value of 3.0 eV [28,55] was used to introduce orbital-dependent corrections for the strong on-site Coulomb repulsion among the localized 3d electrons of Cu in CuO. A 2 × 2 × 1 Monkhorst-Pack k-point mesh was utilized for summations over the Brillouin zone. The kinetic energy cutoff was 400 eV. The convergence criteria for the electronic and ionic relaxation were 10^{-4} eV and 10^{-3} eV $Å^{-1}$, respectively.

3. Results and discussion

3.1. Characterization

The sample of CuO mesoporous nanosheets (denoted as CuO-MNS) was prepared by the reaction between NaOH aqueous solution and copper ammonia complex ($Cu(NH_3)_4^{2+}$) formed by $CuSO_4$ and ammonia aqueous solution at 25 °C (Experimental). XRD reveals that the as-synthesized CuO sample has monoclinic crystalline structure (JCPDS 48-1548) as shown in Fig. 1A. The morphology of the CuO-MNS sample is characterized by SEM and TEM. SEM images indicate that the CuO-MNS sample has morphology of nanosheets with size of hundreds of nanometers and thickness of tens of nanometers (Fig. 1B, Fig. S1). TEM images show that there are numerous mesopores on the surface of a nanosheet (Fig. 1C). HRTEM image on the side of a nanosheet reveals that it has lattice spacing of 0.252 nm corresponding to $\{1\,1\,\bar{1}\}$ facet (Fig. 1D). Lattice spacing of 0.253 nm corresponding to {002} facet (Fig. 1E) and lattice spacing of 0.171 nm corresponding to {020} facet (Fig. 1F) are observed on the surface of a nanosheet by HRTEM. The TEM observation indicates that the CuO-MNS has the exposed $\{1\,1\,\bar{1}\}$ surface. The porous structure of CuO-MNS is confirmed by N_2 adsorption (Fig. 2). The average pore size of CuO-MNS is 5.6 nm, and its total pore volume is 0.22 $cm^3\,g^{-1}$. The BET surface area of CuO-MNS is 30.1 $m^2\,g^{-1}$.

3.2. Photothermocatalytic activity. We tested the photothermocatalytic activity of cuO-MNS for the catalytic oxidation of CO (poisonous air pollutant) as mode reaction under the illumination of a Xe

lamp, which has spectral profile similar to solar spectra [46]. In order to make comparison, the catalytic activity of TiO_2 (P25) (a well-known benchmark photocatalyst) and a commercial nonporous CuO sample with monoclinic crystalline structure (Fig. S2-S3) and BET surface area of 16.7 $m^2\,g^{-1}$ (Fig. S4) under the Xe lamp illumination was tested. The rate of CO_2 production (r_{CO2}) for the samples is compared. Among three samples, TiO_2 (P25) has the lowest catalytic activity. Its CO conversion is 1.0%, and its r_{CO2} is 0.26 μmol min^{-1}. The commercial nonporous CuO sample demonstrates higher catalytic activity. Its CO_2 conversion and r_{CO2} are 4.4%, 1.19 μmol min^{-1}, respectively (Fig. 3A and B). Impressively, CuO-MNS demonstrates the highest catalytic activity. Its CO_2 conversion is 85.1% and its r_{CO2} is very high (23.42 μmol min^{-1}). Compared to TiO_2 (P25) and the commercial nonporous CuO sample, the catalytic activity of CuO-MNS is enhanced by 88.7 and 19.8 times, respectively. As the BET surface area of CuO-MNS (30.1 $m^2\,g^{-1}$) is higher than that of the nonporous commercial CuO (16.7 $m^2\,g^{-1}$), in order to prove if the much higher catalytic activity of CuO-MNS than the nonporous commercial CuO arises from its higher BET surface area, we compared their specific CO_2 production rate per unit area (r_{SCO2}). The r_{SCO2} of CuO-MNS is 7.8 μmol $m^{-2}\,min^{-1}$, which is 11 times higher than that of the nonporous commercial CuO (0.71 μmol $m^{-2}\,min^{-1}$).

The photothermocatalytic durability of CuO-MNS for CO oxidation under the Xe lamp illumination was tested. As shown in Fig. 3C, after continuously reacted for 30 h, the photothermocatalytic activity of CuO-MNS remains unchanged. The result indicates that CuO-MNS has excellent catalytic durability.

We investigated the effect of light intensity on the photothermocatalytic activity of CuO-MNS for CO oxidation under the UV–vis-IR illumination from the Xe lamp. As shown in Fig. S5, with the lower light intensity (237.6 mW cm^{-2}), CuO-MNS demonstrates photothermocatalytic activity with r_{CO2} of 3.34 μmol min^{-1}. With the light intensity increasing from 237.6 to 364.2 and 475.7 mW cm^{-2}, the r_{CO2} of CuO-MNS considerably increases from 3.34 to 15.44 and 23.42 μmol min^{-1}.

We also tested the photothermocatalytic activity of CuO-MNS and the nonporous commercial CuO sample for CO oxidation under the Vis-IR or IR illumination. Under the Vis-IR illumination of λ > 420, 560, and 690 nm, CuO-MNS demonstrates high catalytic activity. Its CO conversion in these cases is 83.9%, 80.2%, 79.0%, respectively (Fig. 4A). Correspondingly, its r_{CO2} is 22.40, 22.05, 21.08 μmol min^{-1}, respectively (Fig. 4B). Even under the λ > 830 nm IR illumination, CuO-MNS still shows good catalytic activity. Its CO conversion is 44.4%, and its r_{CO2} is 12.03 μmol min^{-1}. In striking contrast, under the Vis-IR illumination of λ > 420, 560, and 690 nm, the photothermocatalytic activity of the nonporous commercial CuO sample is much lower than the corresponding that of CuO-MNS. Its CO conversion in these cases is 2.2%, 1.5%, and 0.3%, respectively (Fig. 4A). Correspondingly, its r_{CO2} is 0. 61, 0.41, and 0.09 μmol min^{-1}, respectively (Fig. 4B). Under the λ > 830 nm IR illumination, no detectable CO_2 is detected for the nonporous commercial CuO sample, indicating that it has no IR photothermocatalytic activity.

3.3. Mechanism

To clarify why CuO-MNS demonstrates very good catalytic activity for CO oxidation under the Xe lamp illumination, we tested its optical absorption because it is indispensable for a photocatalytic process. In order to make comparison, the optical absorption of the commercial nonporous CuO sample was also measured. As shown in Fig. 5A, CuO-MNS has strong absorption in the region of entire solar spectrum from 200 to 2400 nm. The commercial nonporous CuO sample also has strong absorption in the region of entire solar spectrum. However, compared to CuO-MNS, the absorption of the commercial nonporous CuO sample is stronger in the IR region of λ > 792 nm. The result suggests that the formation of mesoporous for CuO-MNS causes an alteration in the optical property of CuO.

Whether does the strong absorption of CuO-MNS cause photocatalytic activity according to the conventional photocatalytic mechanism on photocatalysts such as TiO_2? As we all know, conventional photocatalysis is able to occur at ambient temperature, so we tested the photocatalytic activity of CuO-MNS at near ambient temperature under the UV–vis-IR illumination from the Xe lamp. As shown in Fig. 5B, the photocatalytic activity of CuO-MNS has very low. Its r_{CO2} is only 0.07 μmol min^{-1}. This indicates that CuO-MNS is not effective photocatalyst, which is agreement to the result reported [43]. Under the UV–vis-IR illumination with the same light intensity (475.7 mW cm^{-2}),

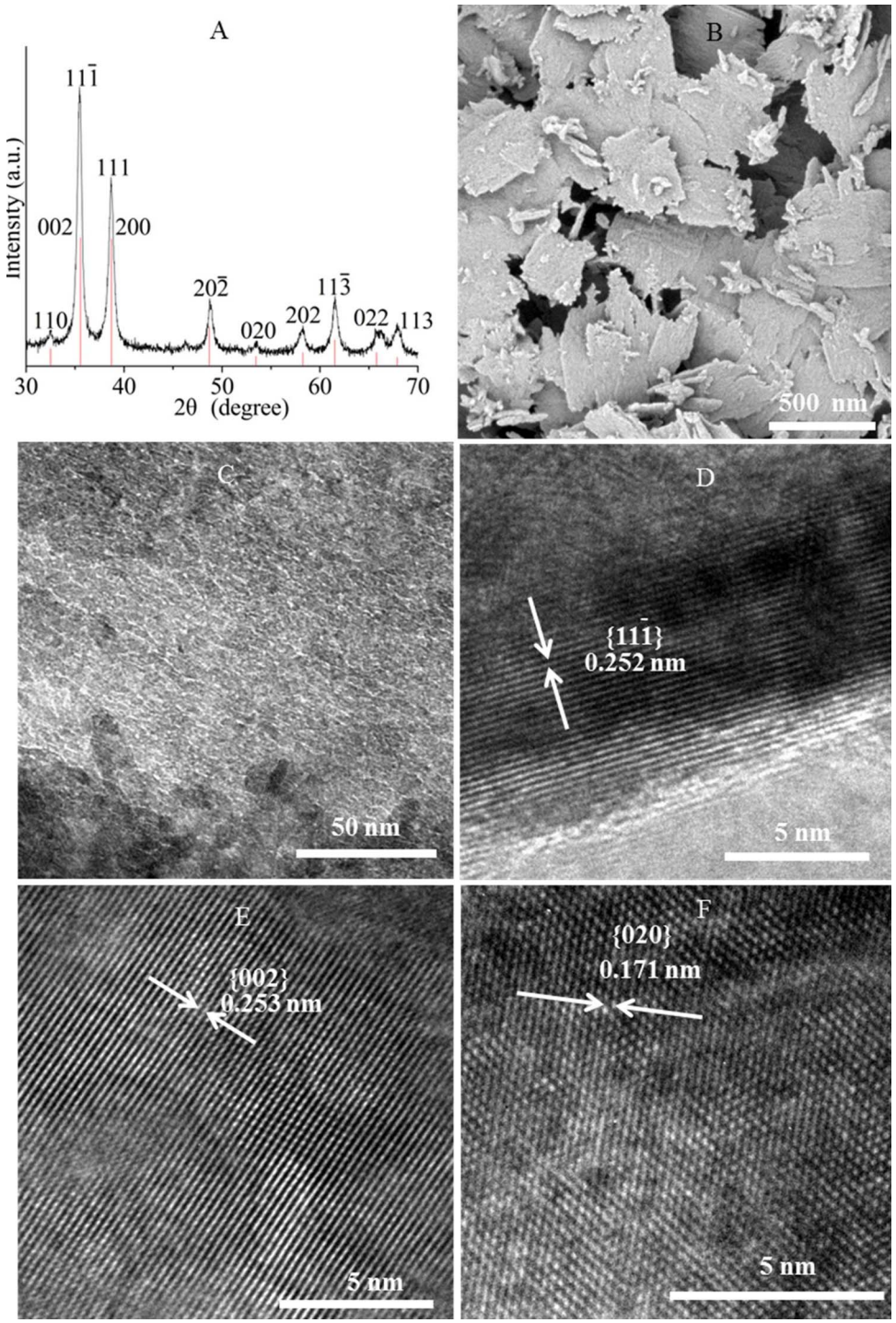

Fig. 1. XRD patterns (A), SEM images (B), TEM images (C), HRTEM image on the side of a nanosheet (D), and HRTEM image (E, F) on the surface of a nanosheet of CuO-MNS: XRD patterns of monoclinic crystalline structure of CuO (JCPDS 48-1548) are indicated by red lines in Fig. 1A. (For interpretation of the references to color in this figure legend, the reader is referred to the web version of this article.)

the photothermocatalytic activity of CuO-MNS (r_{CO2} = 23.42 μmol min^{-1}) is 331 times higher than its conventional photocatalytic activity. This result suggests that the very high photothermocatalytic activity of CuO-MNS under the Xe lamp illumination (Fig. 3) mainly originates from SLD thermocatalytic CO oxidation rather than the conventional photocatalytic CO oxidation: The strong absorption of CuO-MNS leads to an increase in its temperature due to photothermal conversion. When the temperature exceeds the light-off temperature ($T_{light\text{-}off}$) of the thermocatalytic CO oxidation, the reaction takes place.

In order to corroborate the mechanism, the surface temperature of CuO-MNS and the commercial nonporous CuO sample during the photothermocatalytic CO oxidation under the Xe lamp illumination (Fig. 3) were measured. The Xe lamp illumination leads to a quick elevation of the surface temperature of CuO-MNS to an equilibrium temperature (T_{eq}) of 205 °C owing to the photothermal conversion (Fig. 5C). The T_{eq} of the commercial nonporous CuO sample is 218 °C, which is slightly higher than that of CuO-MNS. This is attributed to the stronger optical absorption of the commercial nonporous CuO sample in the IR region of λ > 792 nm than CuO-MNS (Fig. 5A). The surface temperature of CuO-MNS and the commercial nonporous CuO sample during the catalytic CO oxidation under the Vis-IR or IR illumination (Fig. 4) was also measured. Under the Vis-IR or IR illumination of λ > 420, 560, 690, and 830 nm, the T_{eq} of CuO-MNS is 199, 195, 176, and 153 °C, respectively (Fig. 5C). The corresponding T_{eq} of the commercial nonporous CuO sample is 212, 203, 186, and 167 °C, respectively (Fig. 5C). The result indicates that both CuO-MNS and the

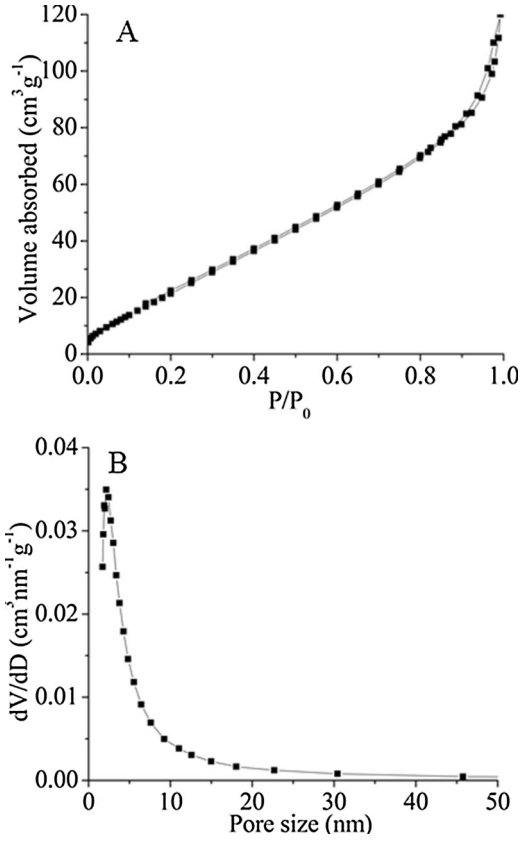

Fig. 2. N_2 adsorption–desorption isotherm (A) and pore size distribution (B) of CuO-MNS.

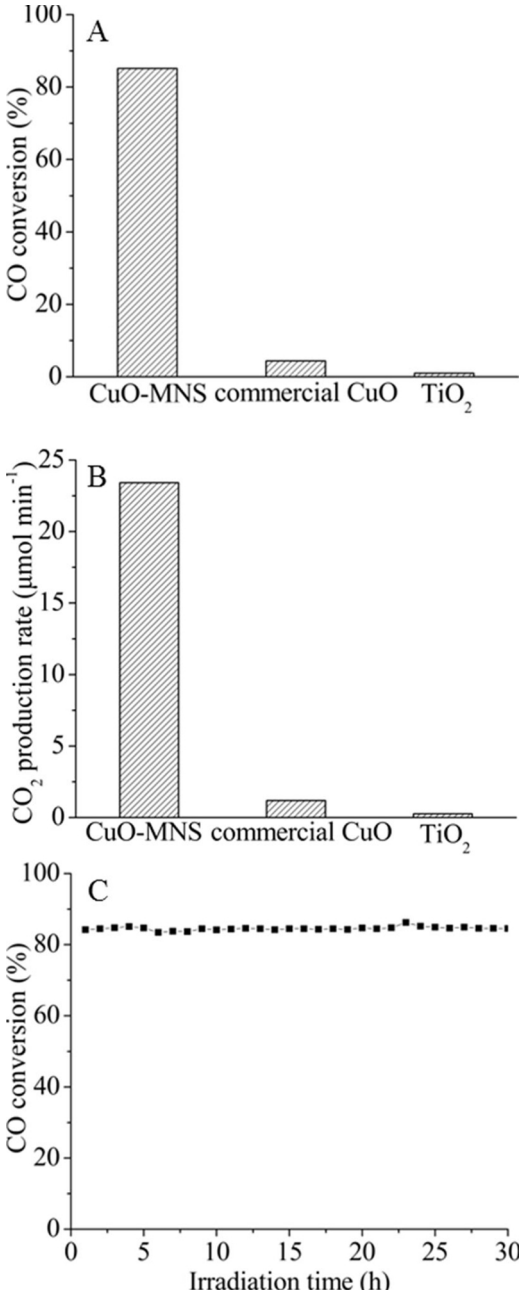

Fig. 3. CO conversion (A) and CO_2 production rate (B) of the samples, and photothermocatalytic durability of CuO-MNS for CO oxidation under the Xe lamp illumination (C).

commercial nonporous CuO sample are able to effectively convert the absorbed UV–vis-IR, Vis-IR or IR energy to thermal energy. The T_{eq} values of the commercial nonporous CuO sample higher than the corresponding values of CuO-MNS are attributed to the stronger optical absorption of the former in the IR region of $\lambda > 792$ nm than the latter (Fig. 5A).

To reveal whether the T_{eq} is able to exceed the $T_{light\text{-}off}$ for the thermocatalytic CO oxidation on CuO-MNS, we tested the thermocatalytic activity of CuO-MNS for CO oxidation at different temperatures in the dark (Experimental). As shown in Fig. 5D, with the elevation of the temperature to 100 °C, CO starts to be oxidized on CuO-MNS ($T_{ligh\text{-}off} = \sim 100$ °C). With the elevation of the reaction temperature from 120 °C, the thermocatalytic activity of CuO-MNS is rapidly enhanced. Its T_{50} and T_{90} (the reaction temperature corresponding to 50% and 90% of CO conversion, respectively) are 176, 200 °C, respectively. All the T_{eq} values of CuO-MNS exceed the $T_{light\text{-}off}$. Therefore, the SLD thermocatalytic CO oxidation on CuO-MNS is able to occur.

As shown in Fig. 5A and C, the nonporous commercial CuO sample has stronger absorption and higher T_{eq} than CuO-MNS. Why does the nonporous commercial CuO sample demonstrate much lower photothermocatalytic activity than CuO-MNS (Fig. 3A and B)? To find out the issue, the thermocatalytic activity of the commercial nonporous CuO sample at the different temperature in the dark was tested under the same reaction condition as that of CuO-MNS. It can be seen from Fig. 5D, the commercial nonporous CuO sample demonstrates much lower thermocatalytic activity. Only with the reaction temperature elevated to ~220 °C can the thermocatalytic CO oxidation take place ($T_{light\text{-}off} = 220$ °C). Its T_{50} is 333 °C, and its T_{90} exceeds 420 °C. Compared to the nonporous commercial CuO sample, the T_{50} and T_{90} of CuO-MNS are tremendously reduced by 157, > 220 °C, respectively. As the T_{eq} value of the nonporous commercial CuO sample under the UV–vis-IR illumination from the Xe lamp (218 °C) is just close to its $T_{light\text{-}off}$ (~220 °C), it exhibits very low photothermocatalytic activity (Fig. 3). The tremendously higher thermocatalytic activity of CuO-MNS than the nonporous commercial CuO sample (Fig. 5D) results in its much higher photothermocatalytic activity (Fig. 3A and B). As all the T_{eq} values of the nonporous commercial CuO sample under the Vis-IR and IR illumination (Fig. 5C) is less than its $T_{light\text{-}off}$ (~220 °C), the solar-light-driven thermocatalytic oxidation of CO on CuO as discussed above does not occur. The very low catalytic activity of the nonporous commercial CuO sample under the Vis-IR illumination (Fig. 4) is due to the photocatalytic oxidation of CO on CuO [1–3,33].

3.4. Origin of the enhanced thermocatalytic activity

Why does CuO-MNS exhibit much higher thermocatalytic activity than the commercial nonporous CuO sample? It is commonly accepted that the catalytic oxidation of reducible compounds (e.g. CO) on CuO

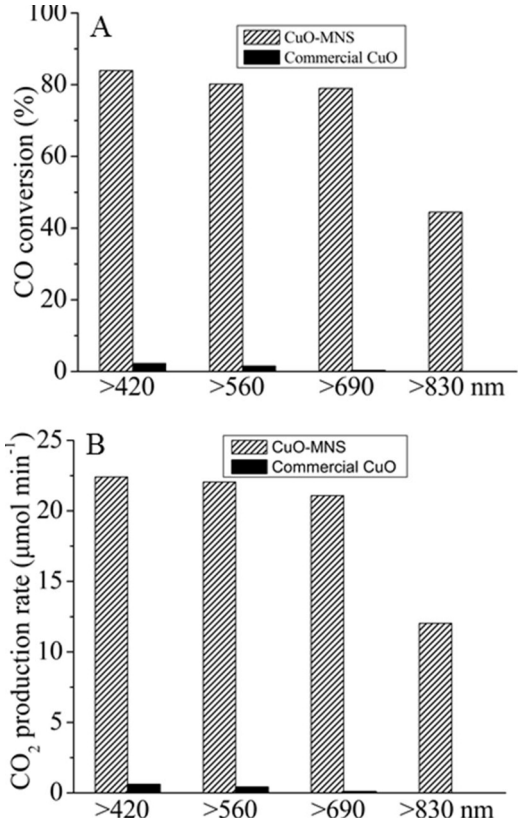

Fig. 4. CO conversion (A) and CO_2 production rate (B) of CuO-MNS and the nonporous commercial CuO sample for CO oxidation under the Vis-IR or IR illumination.

and its composites follows the Mars-van Krevelen mechanism: reducible compounds (e.g. CO) react with the surface lattice oxygen of CuO, and the produced oxygen vacancies on the surface of CuO are subsequently replenished by O_2 [56–58]. The former step of CO oxidation by the lattice oxygen of CuO is believed as a rate-determining step [57,58]:

$$CuO + xCO = CuO_{1-x} + xCO_2 \quad (1)$$

$$CuO_{1-x} + 0{\cdot}5xO_2 = CuO \quad (2)$$

Therefore, we evaluated the activity of the lattice oxygen in the commercial nonporous CuO sample and CuO-MNS by CO-TPR. As shown in Fig. 6A, the commercial nonporous CuO sample has strong CO consumption peak around 336 °C, indicating that it is directly reduced by CO to metallic copper around 336 °C. In striking contrast, compared to the commercial nonporous CuO sample, the strong CO consumption peak of CuO-MNS significantly shifts from 336 to 212 °C. The result indicates that the presence of mesopores in CuO-MNS causes a significant improvement in the lattice oxygen activity of CuO. This accounts for the reason why the CuO-MNS exhibits much higher thermocatalytic activity than the commercial nonporous CuO sample as shown in Fig. 5D.

The activity of the lattice oxygen in CuO-MNS and the commercial nonporous CuO is further studied by Raman. As shown in Fig. 6B, the commercial nonporous CuO sample has a strong Raman peak around 301.7 cm^{-1} and weak Raman peak around 350.0 cm^{-1}. The strong Raman peak around 301.7 cm^{-1} is assigned to A_g mode in which the O atoms vibrate along the *b* axis. The weak Raman peak around 350.0 cm^{-1} corresponds to B_g mode in which the O atoms vibrate approximately along *a* axis [59]. Compared to the commercial nonporous CuO, there is a considerable red shift for the corresponding Raman peaks of CuO-MNS. The strong Raman peak corresponding to A_g mode shifts from 301.7 to 292.0 cm^{-1}. The weak Raman peak corresponding to B_g mode shifts from 350.0 to 343.5 cm^{-1}. Based on the Raman shift of A_g mode, we estimated the Cu—O bond force constant (k) of the two CuO samples according to the Hooke's law [60,61].

$$\omega = \frac{\sqrt{k/\mu}}{2\pi c}$$

Where ω is the Raman shift (cm^{-1}), c is light velocity, μ is effective mass.

The *k* of Cu—O corresponding to the strong Raman peak (A_g mode)

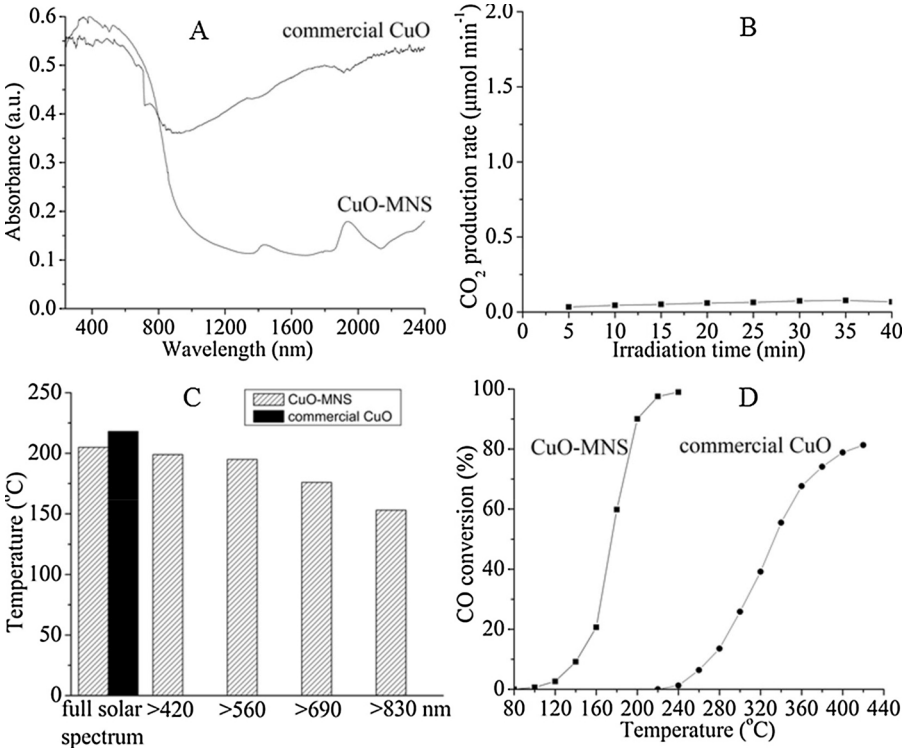

Fig. 5. Reflectance diffusive absorption of CuO-MNS and commercial nonporous CuO (A); photocatalytic activity of CuO-MNS for CO oxidation at near room temperature (B); Equilibrium temperature of the CuO samples under the UV–vis-IR, Vis-IR, or IR illumination; Thermocatalytic activity of the CuO samples for CO oxidation at different temperature in the dark (D).

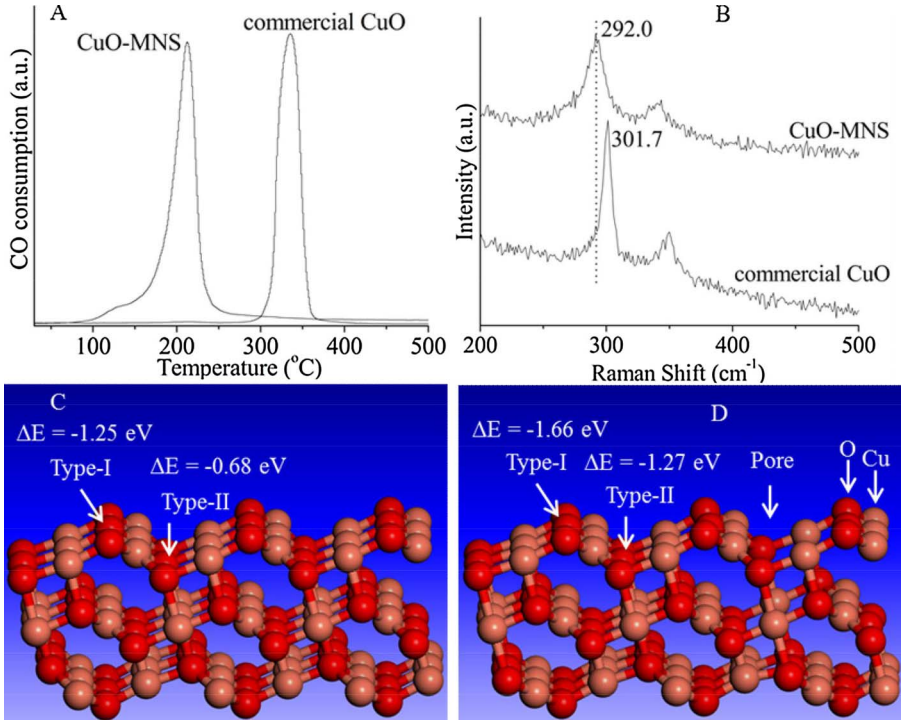

Fig. 6. CO-TPR profile (A) and Raman spectra (B) of CuO-MNS and the commercial nonporous CuO sample; The calculated slabs of $Cu_{54}O_{54}$ without nanopore (C) and $Cu_{52}O_{52}$ with nanopore (pore size: ~0.58 nm) (D): the oxygen atom pointed by arrow represents the oxygen to be reacted with CO.

in CuO-MNS is 63.9 N m^{-1}, which is lower than that in the commercial nonporous CuO (68.3 N m^{-1}). This result suggests that the Cu—O bond strength in CuO-MNS is less than that in the commercial nonporous CuO. This means that the presence of mesopores in CuO-MNS results in the improvement of lattice oxygen activity, thus significantly enhancing the thermocatalytic activity of CuO, which is in agreement to the result by CO-TPR.

To provide more evidence to the experimental conclusion by CO-TPR and Raman, the effect of the mesopore formation on the lattice oxygen activity of CuO is theoretically studied by DFT calculations. As the CuO-MNS have the exposed {1 1 $\bar{1}$} surface as observed by HRTEM in Fig. 1, we constructed a $Cu_{54}O_{54}$ slab of 3 CuO layers and 3 × 3 {1 1 $\bar{1}$} surface with monoclinic tenorite structure (JCPDS 48-1548) for the DFT calculations (Fig. 6C). The space between neighboring {1 1 $\bar{1}$} surfaces of the slabs was 1.0 nm. A $Cu_{52}O_{52}$ slab with a nanopore (pore size: ~0.58 nm) on its {1 1 $\bar{1}$} surface is constructed by the removal of Cu_2O_2 cluster from the $Cu_{54}O_{54}$ slab (Fig. 6D). We calculated the energy of CO reacting with one oxygen atom from the surface of the two slabs (ΔE):

$$Cu_{54}O_{54} + CO = Cu_{54}O_{53} + CO_2$$

$$Cu_{52}O_{52} + CO = Cu_{52}O_{51} + CO_2$$

$$\Delta E = E_{SOV} + E_{CO2} - E_S - E_{CO}$$

Where E_{SOV} is the energy of the slab with one oxygen vacancy, E_S is the energy of the slab; E_{CO2} or E_{CO} is the energy of CO_2 or CO molecule in gas phase, respectively. The slabs are used as initial configurations for structural optimization. The ΔE of CO reacting with one type-I oxygen atom on the $Cu_{54}O_{54}$ slab without a nanopore is −1.25 eV (Fig. 6C). In striking contrast, the ΔE of CO reacting with the corresponding type-I oxygen atom around the nanopore of the $Cu_{52}O_{52}$ slab with a nanopore reduces to −1.66 eV (Fig. 6D). Similarly, the ΔE of CO reacting with one type-II oxygen atom on the $Cu_{54}O_{54}$ slab without a nanopore is −0.68 eV (Fig. 6C). The ΔE of CO reacting with the corresponding type-II oxygen atom around the nanopore of the $Cu_{52}O_{52}$ slab with a nanopore reduces to −1.27 eV (Fig. 6D). The result of the DFT calculations indicates that the formation of nanopore on the surface of CuO considerably improves the activity of the surface lattice oxygen around the nanopore. This is in a good agreement to the results by CO-TPR and Raman.

3.5. Novel photoactivation

Whether does the greatly effective photothermocatalytic activity of CuO-MNS (Fig. 3) merely originate from the SLD thermocatalysis? If yes, at the same reaction temperature, the catalytic activity of CuO-MNS in the dark should be the same as that with the Xe lamp illumination. To find out this question, we tested the catalytic activity of CuO-MNS for CO oxidation in the dark or with the Xe lamp illumination under the otherwise identical reaction condition (see Experimental). As shown in Fig. 7, at the same reaction temperature above 120 °C, compared to the catalytic activity of CuO-MNS in the dark, the Xe illumination considerably promotes its catalytic activity. The result clearly reveals the existence of a photoactivation effect for CO oxidation on CuO-MNS to improve its SLD thermocatalytic activity as CuO-MNS has no detectable photocatalytic activity under the Xe lamp illumination at near room temperature (Fig. 5B).

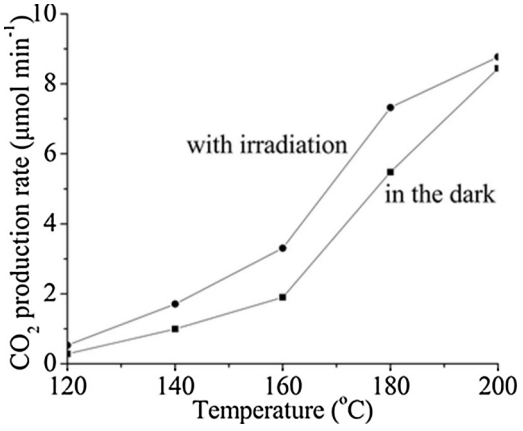

Fig. 7. The catalytic activity of CuO-MNS for CO oxidation at the different temperature in the dark or with the Xe lamp illumination.

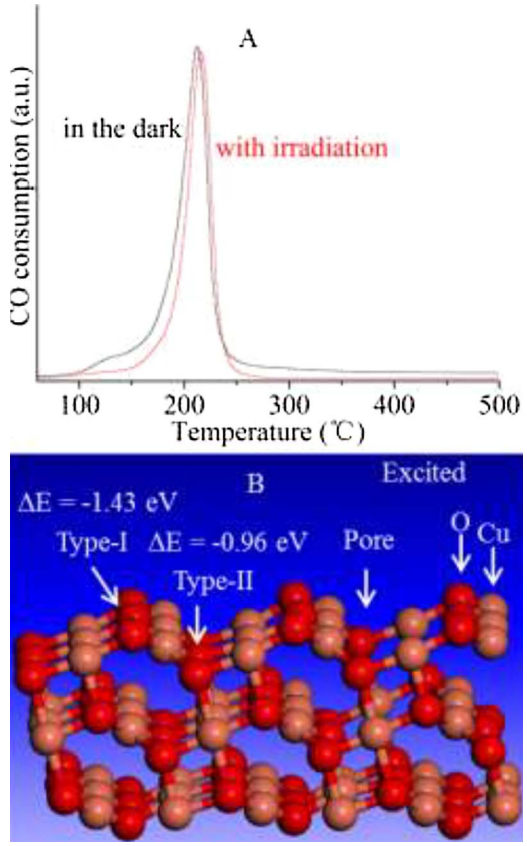

Fig. 8. CO-TPR profile of CuO-MNS in the dark and with the Xe lamp illumination (A); the calculated slabs of $Cu_{52}O_{52}$ with nanopore in the excited stat (B): the oxygen atom pointed by arrow represents the oxygen to be reacted with CO.

3.5.1. CO-TPR

As the lattice oxygen activity of CuO plays an important role in its thermocatalytic activity [56–58] as discussed above, the effect of the Xe illumination on the lattice oxygen activity of CuO-MNS is investigated to put more physical insight in the novel photoactivation. CO-TPR of the CuO-MNS sample in the dark and with the Xe lamp illumination under the otherwise identical condition was performed. As shown in Fig. 8A, compared to the CO-TPR profile of CuO-MNS in the dark, the Xe lamp illumination causes a slight shift of the maximum CO consumption peak temperature to higher temperature, suggesting that the illumination causes a slight reduction in the lattice oxygen activity of CuO-MNS.

To further affirm the conclusion by CO-TPR, the effect of the illumination on the lattice oxygen activity of CuO is theoretically investigated by DFT calculations. The optical absorption of CuO causes the excitation of 3*d* electrons of Cu ions [33], which results in the change in the number of electrons in up and down spin component for CuO. The ΔE of CO reacting with one lattice oxygen from $Cu_{52}O_{52}$ slab with a nanopore in excited state (Fig. 8B) is calculated by a constrained occupancy approach of DFT through setting the excitation of one *d* electron to the excited state by changing the electron number of up and down spin component [55,62]. In the case, the excitation of both CO and CO_2 molecules is not considered because they are unable to be excited by the solar light illumination.

$$Cu_{52}O_{52}^{*}\ (\text{excited}) + CO = CO_2 + Cu_{52}O_{51}^{*}(\text{excited})$$

$$\Delta E = E_{Cu52O51^{*}} + E_{CO2} - E_{Cu52O52^{*}} - E_{CO}$$

Compared to the corresponding ΔE value in the ground state (-1.66 eV), the ΔE of CO reacting with type-I lattice oxygen from $Cu_{52}O_{52}$ slab in the excited state increases to -1.43 eV. Similarly, the ΔE of CO reacting with type-II lattice oxygen from $Cu_{52}O_{52}$ slab in the excited state considerably increases from -1.27 (in the ground state) to -0.96 eV (Fig. 8B). The DFT calculation reveals that the illumination reduces the lattice oxygen activity of $Cu_{52}O_{52}$, which is in accordance to the experimental result by CO-TPR.

According to the Mars-van Krevelen mechanism as discussed above, the results of CO-TPR and DFT calculation mean that the illumination should seem to cause a reduction in the catalytic activity of Cu-MNS, which is completely opposite to our observation of the considerable catalytic enhancement upon the illumination as shown in Fig. 7. The result of the reduction in the lattice oxygen activity of CuO-MNS upon the illumination is also completely opposite to the result for manganese oxide reported in recent work,[45] in which the illumination causes a considerable enhancement in the lattice oxygen activity of manganese oxide, thus improving its catalytic activity.[45] The CO-TPR result suggests that the novel photoactivation of the catalytic enhancement upon the illumination (Fig. 7) maybe derives from the effect of the illumination on the re-oxidation of the reduced cupric oxide (CuO_{1-x}) in accordance to the Mars-van Krevelen mechanism as discussed above.

3.5.2. O_2-TPO

In order to show whether the illumination could accelerate the re-oxidation of the reduced cupric oxide (CuO_{1-x}) according to the Mars-van Krevelen mechanism, O_2-TPO of the CuO-MNS sample pre-reduced by 5 vol% CO/He in the dark and with the Xe lamp illumination under the otherwise identical condition was performed (see Experimental). As shown in Fig. 9A, compared to the O_2-TPO profile of the pre-reduced CuO-MNS sample in the dark, the two maximum O_2 consumption peaks obviously shift to lower temperatures upon the Xe lamp illumination. The result reveals that the Xe lamp illumination accelerates the re-oxidation of the pre-reduced CuO-MNS sample, thus improving the catalytic activity of CuO-MNS (Fig. 7).

To affirm the O_2-TPO result, the effect of the illumination on the re-oxidation of the reduced cupric oxide is theoretically studied by DFT calculation. The ΔE of O_2 replenishing one oxygen vacancy from $Cu_{52}O_{51}$ slab with a nanopore in excited state (Fig. 9B–E) is calculated by a constrained occupancy approach of DFT through setting the excitation of one *d* electron to the excited state by changing the electron number of up and down spin component [62]. In the case, the excitation of O_2 molecule is not considered because it is unable to be excited by the solar light illumination.

$$Cu_{52}O_{51}^{*}\ (\text{excited}) + 0.5O_2 = Cu_{52}O_{52}^{*}(\text{excited})$$

$$\Delta E = E_{Cu52O52^{*}} - 0.5\,E_{O2} - E_{Cu52O51^{*}}$$

Compared to the corresponding ΔE value in the ground state (-1.61 eV), the ΔE of O_2 replenishing type-I oxygen vacancy from $Cu_{52}O_{51}$ slab in the excited state considerably reduces to -1.84 eV (Fig. 9B and C). Similarly, the ΔE of O_2 replenishing type-II oxygen vacancy from $Cu_{52}O_{51}$ slab considerably reduces from -2.00 eV (in the ground state) to -2.31 eV (Fig. 9D and E). The DFT calculation reveals that the illumination accelerates the re-oxidation of $Cu_{52}O_{51}$ to $Cu_{52}O_{52}$, which is in accordance to the experimental result by O_2-TPO.

4. Conclusion

The sample of CuO mesoporous nanosheets (CuO-MNS) was prepared by a facile and novel method of the reaction between NaOH and copper ammonia complex aqueous solution at 25 °C. Remarkably, CuO-MNS demonstrates greatly effective photothermocatalytic activity for CO oxidation under the UV–vis-IR illumination or even under the $\lambda > 830$ nm IR illumination. It is found that the formation of mesopores in CuO-MNS significantly improves the lattice oxygen activity of CuO, thus significantly enhancing the photothermocatalytic activity of CuO. Compared to commercial nonporous CuO, the photothermocatalytic activity of CuO-MNS is enhanced by 19.8 times. The

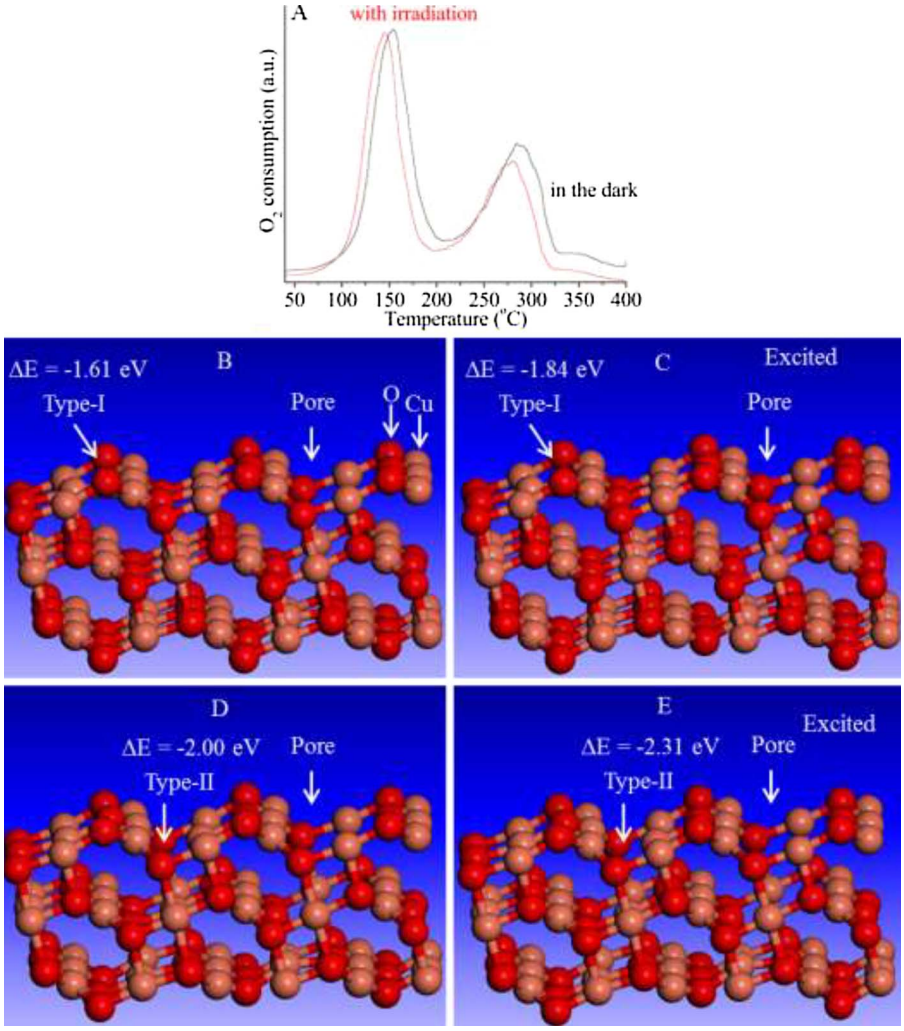

Fig. 9. O_2-TPO profile of the CuO-MNS sample pre-reduced by CO in the dark or with the Xe lamp illumination (A); The calculated slabs of $Cu_{52}O_{51}$ with nanopore and different type of oxygen vacancy on the ground state (B, D) and the excited stat (C, E): the oxygen vacancy pointed by arrow represents the oxygen vacancy to be replenished by O_2.

greatly effective photothermocatalytic activity of CuO-MNS is attributed to effective SLD thermocatalytic CO oxidation. Very interestingly, it is discovered that the SLD thermocatalytic activity of CuO-MNS is considerably promoted by a novel photoactivation: the Xe lamp illumination considerably accelerates the re-oxidation of the reduced CuO-MNS sample, thus considerably enhancing the catalytic activity of CuO-MNS. The present work provides a novel strategy for significantly improving catalytic activity of CuO by designing CuO mesoporous nanosheets. As the concentrated solar light with relatively low solar concentration ratio (less than 5 suns in the present work) can be conveniently obtained by using commercial solar concentrator with very low cost, the present work provides a strategy of effectively utilizing inexhaustible solar energy for environmental abatement.

Acknowledgements

This work was supported by National Natural Science Foundation of China (21473127, 21673168). DFT calculations were performed on Shanghai Supercomputer Center (SSC), China.

Appendix A. Supplementary data

Supplementary data associated with this article can be found, in the online version, at https://doi.org/10.1016/j.apcatb.2017.11.081.

References

[1] X.B. Chen, S.S. Mao, Chem. Rev. 107 (2007) 2891–2959.
[2] Y.H. Zhang, Z.R. Tang, X.Z. Fu, Y.J. Xu, Appl. Catal. B 3–4 (2011) 445–452.
[3] L. Ren, Y.Z. Li, J.T. Hou, J.L. Bai, M.Y. Mao, M. Zeng, X.J. Zhao, Appl. Catal. B 181 (2016) 625–634.
[4] H.J. Yu, R. Shi, Y.X. Zhao, T. Bian, Y.F. Zhao, C. Zhou, G.I.N. Waterhouse, L.Z. Wu, C.H. Tung, T.R. Zhang, Adv. Mater. 29 (2017) 1605148.
[5] Y.F. Zhao, B. Zhao, J.J. Liu, G.B. Chen, R. Gao, S.Y. Yao, M.Z. Li, Q.H. Zhang, L. Gu, J.L. Xie, X.D. Wen, L.Z. Wu, C.H. Tung, D. Ma, T.R. Zhang, Angew. Chem. Int. Ed. 55 (2016) 4215–4219.
[6] R. Shi, Y.H. Cao, Y.J. Bao, Y.F. Zhao, G.I.N. Waterhouse, Z.Y. Fang, L.Z. Wu, C.H. Tung, Y.D. Yin, T.R. Zhang, Adv. Mater. 29 (2017) 1700803.
[7] J. Chen, D.M. Zhao, Z.D. Diao, M. Wang, S.H. Shen, Sci. Bull. 61 (2016) 292–301.
[8] C. Han, Q. Quan, H.M. Chen, Y.G. Sun, Y.J. Xu, Small 13 (2017) 1602947.
[9] Y.H. Sang, H. Liu, A. Umar, Chemcatchem 7 (2015) 559–573.
[10] Y. Tang, W.H. Di, X.S. Zhai, R.Y. Yang, W.P. Qin, ACS Catal. 3 (2013) 405–412.
[11] C.H. Li, F. Wang, J. Zhu, J.C. Yu, Appl. Catal. B 100 (2010) 433–439.
[12] W.P. Qin, D.S. Zhang, D. Zhao, L.L. Wang, K.Z. Zheng, Chem. Commun. 46 (2010) 2304–2306.
[13] Z.X. Li, F.B. Shi, T. Zhang, H.S. Wu, L.D. Sun, C.H. Yan, Chem. Commun. 47 (2011) 8109–8111.
[14] J.M. Zhang, Y. Huang, L. Jin, F. Rosei, F. Vetrone, J.P. Claverie, ACS Appl. Mater. Interfaces 9 (2017) 8142–8150.
[15] S.Q. Huang, L. Gu, C. Miao, Y. Lou, N.W. Zhu, H.P. Yuan, A.D. Shan, J. Mater. Chem. A 1 (2013) 7874.
[16] W. Wang, W.J. Huang, Y.R. Ni, C.H. Lu, Z.Z. Xu, ACS Appl. Mater. Interfaces 6 (2014) 340–348.
[17] J. Tian, Y.H. Leng, Z.H. Zhao, Y. Xia, Y.H. Sang, P. Hao, J. Zhan, M.C. Li, H. Liu, Nano Energy 11 (2015) 419–427.
[18] H.T. Li, R.H. Liu, Y. Liu, H. Huang, H. Yu, H. Ming, S.Y. Lian, S.T. Lee, Z.H. Kang, J. Mater. Chem. 22 (2012) 17470.
[19] M.C. Ortega-Liebana, J.L. Hueso, R. Arenalc, J. Santamaria, Nanoscale 9 (2017) 1787–1792.
[20] J.B. Cui, Y.J. Li, L. Liu, L. Chen, J. Xu, J.W. Ma, G. Fang, E.B. Zhu, H. Wu, L.X. Zhao,

L.Y. Wang, Y. Huang, Nano Lett. 15 (2015) 6295–6301.
[21] W.Y. Jiang, S. Bai, L.M. Wang, X.J. Wang, L. Yang, Y.R. Li, D. Liu, X.N. Wang, Z.Q. Li, J. Jiang, Y.J. Xiong, Small 12 (2016) 1640–1648.
[22] Z.K. Zheng, T. Tachikawa, T. Majima, J. Am. Chem. Soc. 137 (2015) 948–957.
[23] R.Y. Yan, M. Chen, H. Zhou, T. Liu, X.W. Tang, K. Zhang, H.X. Zhu, J.H. Ye, D. Zhang, T.X. Fan, Sci. Rep. 6 (2016) 20001.
[24] X.H. Zhang, T.Y. Peng, L.J. Yu, R.J. Li, Q.Q. Li, Z. Li, ACS Catal. 5 (2015) 504–510.
[25] X.H. Zhang, L.J. Yu, C.S. Zhuang, T.Y. Peng, R.J. Li, X.G. Li, ACS Catal. 4 (2014) 162–170.
[26] J. Tian, Y.H. Sang, G.W. Yu, H.D. Jiang, X.N. Mu, H. Liu, Adv. Mater. 25 (2013) 5075–5080.
[27] Y.H. Sang, Z.H. Zhao, M.W. Zhao, P. Hao, Y.H. Leng, H. Liu, Adv. Mater. 27 (2015) 363–369.
[28] G. Wang, B.B. Huang, X.C. Ma, Z.Y. Wang, X.Y. Qin, X.Y. Zhang, Y. Dai, M.H. Whangbo, Angew. Chem. Int. Ed. 52 (2013) 1–5.
[29] Z.J. Li, Y. Dai, X.C. Ma, Y.T. Zhu, Phys. Chem. Chem. Phys. 16 (2014) 3267–3273.
[30] Z.J. Zhang, W.Z. Wang, Dalton. Trans. 42 (2013) 12072–12074.
[31] J. Tao, D. Ying, W. Wei, X.C. Ma, B.B. Huang, Phys. Chem. Chem. Phys. 16 (2014) 18596–18604.
[32] C. Pak, J.Y. Woo, K. Lee, W.D. Kim, Y. Yoo, D.C. Lee, J. Phys. Chem. C 116 (2012) 25407–25414.
[33] Q.B. Zhang, K.L. Zhang, D.G. Xu, G.C. Yang, H. Huang, F.D. Nie, C.M. Liu, S.H. Yang, Progr. Mater. Sci. 60 (2014) 208–337.
[34] R. Katwal, H. Kaur, G. Sharma, M. Naushad, D. Pathania, J. Ind. Eng. Chem. 31 (2015) 173–184.
[35] H. Deol, S. Pramanik, M. Kumar, I.A. Khan, V. Bhalla, ACS Catal. 6 (2016) 3771–3783.
[36] X. Liu, Z. Li, Q. Zhang, F. Li, T. Kong, Mater. Lett. 72 (2012) 49–52.
[37] S. Sun, X. Zhang, J. Zhang, L. Wang, X. Song, Z. Yang, Cryst. Eng. Commun. 15 (2013) 867–877.
[38] Y.Z. Fan, R.M. Liu, W. Du, Q.Y. Lu, H. Pang, F. Gao, J. Mater. Chem. 22 (2012) 12609–12617.
[39] L.F. Yang, D.Q. Chu, L.M. Wang, Mater. Lett. 160 (2015) 246–249.
[40] J. Liu, J. Jin, Z. Deng, S.Z. Huang, Z.Y. Hua, L. Wang, C. Wang, L.H. Chen, Y. Li, G. Van Tendeloo, B.L. Su, J Colloid Interface Sci. 384 (2012) 1–9.
[41] Y. Li, X.Y. Yang, J. Rooke, G.Van Tendeloo, B.L. Su, J. Colloid Interface Sci. 348 (2010) 303–312.
[42] B. Shaabani, E. Alizadeh-Gheshlaghi, Y. Azizian-Kalandaragh, A. Khodayari, Adv. Powder Technol. 25 (2014) 1043–1052.
[43] M. Miyauchi, A. Nakajima, T. Watanabe, K. Hashimoto, Chem. Mater. 14 (2002) 2812–2818.
[44] M.Y. Mao, Y.Z. Li, J.T. Hou, M. Zeng, X.J. Zhao, Appl. Catal. B 174 (2015) 496–503.
[45] F. Liu, M. Zeng, Y.Z. Li, Y. Yang, M.Y. Mao, X.J. Zhao, Adv. Funct. Mater. 26 (2016) 4518–4526.
[46] J.T. Hou, Y.Z. Li, M.Y. Mao, Y.Z. Yue, G.N. Greaves, X.J. Zhao, Nanoscale 7 (2015) 2633–2640.
[47] Y.L. Zheng, W.Z. Wang, D. Jiang, L. Zhang, X.M. Li, Z. Wang, J. Mater. Chem. A 4 (2016) 105–112.
[48] D. Jiang, W.Z. Wang, E. Gao, L. Zhang, S.M. Sun, J. Phys. Chem. C 117 (2013) 24242–24249.
[49] J.L. Fang, D.Z. Li, Y. Shao, J.H. Hu, J. Mater. Chem. A 4 (2016) 14213–14221.
[50] M.Y. Mao, Y.Z. Li, H.Q. Lv, J.T. Hou, M. Zeng, L. Ren, H. Huang, X.J. Zhao, Environ. Sci. Nano 4 (2017) 373–384.
[51] J. Xu, X. Li, X. Wu, W.Z. Wang, R. Fan, X.K. Liu, H.L. Xu, J. Phys. Chem. C 120 (2016) 12666–12672.
[52] J.T. Hou, L.L. Liu, Y.Z. Li, M.Y. Mao, H.Q. Lv, X.J. Zhao, Environ. Sci. Technol. 47 (2013) 13730–13736.
[53] P.E. Blochl, Phys. Rev. B 50 (1994) 17953–17979.
[54] G. Kress, J. Hafner, Phys. Rev. B 48 (1993) 13115–13118.
[55] M. Zeng, Y.Z. Li, F. Liu, Y. Yang, M.Y. Mao, X.J. Zhao, Appl. Catal. B 200 (2017) 521–529.
[56] H.Z. Bao, W.H. Zhang, Q. Hua, Z.Q. Jiang, J.L. Yang, W.X. Huang, Angew. Chem. Int. Ed. 50 (2011) 12294–12298.
[57] A.P. Jia, G.S. Hu, L. Meng, Y.L. Xie, J.Q. Lu, M.F. Luo, J. Catal. 289 (2012) 199–209.
[58] A. Martínez-Arias, M. Fernández-García, O. Gálvez, J.M. Coronado, J.A. Anderson, J.C. Soria, J. Conesa, G. Munuera, J. Catal. 195 (2000) 207–216.
[59] L. Debbichi, M.C. Marco de Lucas, J.F. Pierson, P. Kruger, J. Phys. Chem. C 116 (2012) 10232–10237.
[60] Y.J. Wei, L.Y. Yan, C.Z. Wang, X.G. Xu, F. Wu, G. Chen, J. Phys. Chem. B 108 (2004) 18547–18551.
[61] J.T. Hou, Y.Z. Li, L.L. Liu, L. Ren, X.J. Zhao, J. Mater. Chem. A 1 (2013) 6736–6741.
[62] A. Canning, A. Chaudhry, R. Boutchko, N. Gronbech-Jensen, Phys. Rev. B 83 (2011) 125115.